Electrical characteristics of mixed Zr–Si oxide thin films prepared by ion beam induced chemical vapor deposition at room temperature

F.J. Ferrer [a,*], F. Frutos [b], J. García-López [a], C. Jiménez [c], F. Yubero [d]

[a] Centro Nacional de Aceleradores (CSIC – U. Sevilla), Av. Thomas A. Edison 7, E-41092 Sevilla, Spain
[b] E.T.S. de Ingeniería Informática, Avda. Reina Mercedes s/n, E-41012 Sevilla, Spain
[c] Laboratoire de Matériaux et de Genie Physique, BP 257 – INPGrenoble Minatec – 3 parvis Louis Néel – 38016 Grenoble, France
[d] Instituto de Ciencia de Materiales de Sevilla (CSIC – U. Sevilla), c/ Américo Vespucio 49, E-41092 Sevilla, Spain

Keywords:
Zr-Si oxides
Thin films
Ion beam induced chemical vapor deposition
Static permittivity
Conduction mechanisms
Dielectric breakdown

Mixed Zr–Si oxide thin films have been prepared at room temperature by ion beam decomposition of organometallic volatile precursors. The films were flat and amorphous. They did not present phase segregation of the pure single oxides. A significant amount of impurities (–C–, –CH_x, –OH, and other radicals coming from partially decomposed precursors) remained incorporated in the films after the deposition process. This effect is minimized if the Ar content in the O_2/Ar bombarding gas is maximized. Static permittivity and breakdown electrical field of the films were determined by capacitance–voltage and current–voltage electrical measurements. It is found that the static permittivity increases non-linearly from ~4 for pure SiO_2 to ~15 for pure ZrO_2. Most of the dielectric failures in the films were due to extrinsic breakdown failures. The maximum breakdown electrical field decreases from ~10.5 MV/cm for pure SiO_2 to ~45 MV/cm for pure ZrO_2. These characteristics are justified by high impurity content of the thin films. In addition, the analysis of the conduction mechanisms in the formed dielectrics is consistent to Schottky and Poole-Frenkel emission for low and high electric fields applied, respectively.

1. Introduction

The continuous downscaling of advanced integrated circuits requires the reduction of the gate oxide thickness in metal-oxide-semiconductor (MOS) devices. Today, in conventional SiO_2 based MOS devices, it has been reached the limit in which the leakage current between the gate and the substrate presents a major concern. The substitution of SiO_2 by other dielectrics with higher permittivity and good electrical isolation characteristics will allow the use of higher physical thickness and reduce the leakage current. Among other candidates, ZrO_2 [1] and mixed Zr–Si oxides are currently investigated for this purpose due to their electrical performances [2] and also because they are thermodynamically stable when in contact with silicon [3]. In this context, obtaining flat, compact and amorphous films at room temperature is specially indicated. It is also worth mentioning that ZrO_2 has been proposed to be integrated as high permittivity (high-k) gate dielectric into molecular transistors [4].

The use of ion beams to assist the growth of oxide dielectric materials by the decomposition of volatile precursors leads to the formation of amorphous, compact and smooth thin films [5]. However, if the deposition is performed at room temperature, impurities (–C–, –CH_x, –OH, and other radicals coming from partially decomposed precursors) could be incorporated into the films. The presence of these impurities may influence the ideal electrical performance of the final devices.

In this paper we report on the electrical characteristics of mixed Zr–Si oxide thin films produced by ion beam induced chemical vapor deposition (IBICVD) at room temperature. This technique has been previously used to produce the single SiO_2 [6,7] and ZrO_2 [8] oxides and other mixed oxide as titanium aluminates [9] or titanium silicates [10]. The permittivity and band gap energies in the mixed oxides have been correlated to their local structure. On the other hand, the dielectric strength of the films as well as the deviations of the typical MOS capacitance–voltage characteristic have been correlated to the presence of impurities linked to the preparation procedure. In addition the conduction mechanisms have been identified.

2. Experimental details

Mixed Zr–Si oxide thin films ($Zr_xSi_{1-x}O_2$ with $0<x<1$) have been prepared at room temperature by ion assisted decomposition of triethoxysilane $(CH_3CH_2O)_3SiH$ (TrEOS) and zirconium tetra-tert-butoxide $Zr[OC(CH_3)_3]_4$ (ZTB) volatile precursors. These precursors are extensively used in the literature to grow pure silicon oxide, zirconium oxide and zirconium silicates due to their high vapour pressure at room temperature [10–13]. They were dosed into the reactor (base pressure ~1×10^{-4} Pa) using leak valves with partial

* Corresponding author. Present address: Institut d'Electronique, de Microélectronique et de Nanotechnologie, Av. Poincaré, BP 60069, 59652 Villeneuve d'Ascq cedex, France.
E-mail address: fjferrer@us.es (F.J. Ferrer).

pressures in the range between 5×10^{-4} to 2×10^{-3} Pa. A broad ion beam source (HFQ 1303-3), excited by a RF discharge of O_2/Ar mixtures at about 1×10^{-1} Pa total pressure, was used to supply bombarding ions with 400 eV. The partial pressure ratio of the of the bombarding gases $P_{Ar}/(P_{Ar}+P_{O2})$ was set to 0.85. The ion beam current density measured at the sample position was about 5–10 μA/cm^2. In these conditions, the deposition rate was ~1 nm/min. Thin films with thicknesses in the range of 50 to 400 nm were produced. More experimental details regarding the deposition technique can be found elsewhere [5,14].

Thin film composition was obtained by combined ion beam analysis (IBA) techniques using the 3 MV tandem accelerator of National Center for Accelerators (Seville, Spain). Rutherford backscattering spectrometry (RBS) was used for absolute Zr, Si and Ar quantification using $^4He^{2+}$ or $^4He^{+}$ beams with energies from 1.0 to 3.0 MeV with a surface barrier detector set at 165°. The absolute amount of carbon and oxygen was determined by nuclear reaction analysis using $^{16}O(d,p_1)^{17}O$ and $^{12}C(d,p)^{13}C$, with energies 890 and 980 keV respectively, with a surface barrier detector set at 150° and a 13 μm Mylar filter to avoid that backscattered deuterons reach the detector. For the H quantification we used elastic recoil detection analysis with a 3.0 MeV $^4He^{2+}$ beam, with a surface barrier detector set at 35° and a 13 μm Mylar filter to stop the scattered alpha particles.

Fourier transform infrared (FTIR) spectra were collected in transmission at normal geometry under dry nitrogen atmosphere in a Nicolet 510 spectrometer with an energy resolution of 0.15 cm^{-1}. Double side polished intrinsic Si(100) wafers (resistivity>5000 Ω cm) were used as substrates for this analysis to avoid absorption in the infrared region. The microstructure of the films was examined by scanning electron microscopy (Hitachi FEGSEM S-5200, 5 kV operating voltage). Surface roughness was evaluated with atomic force microscopy (AFM) with a Nanotec apparatus working in non-contact mode. X-ray reflectivity (XRR) characterization was performed with a Siemens D5000 diffractometer using a standard Cu anode. XRR simulations were performed with a REFSIM code supplied by Siemens.

Surface chemical analysis of the thin films was performed by means of X-ray photoelectron spectroscopy (XPS). Photoelectrons were detected with a PHOIBOS100-5MCD electron spectrometer using an unmonochromatised Al K_α excitation source and 40 eV pass energy. With the same apparatus, reflection electron energy loss spectroscopy (REELS) measurements were performed using 1500 eV electrons. The band gap energy E_g of the samples was obtained after analysis of the REELS spectra using OPTEELS software [15].

The capacitance–voltage (C–V) and current–voltage (I–V) characteristics of the films were evaluated on mixed Zr–Si oxide films deposited on polished *n*-type Si(100) wafers with an electrical resistivity of 1–5 Ω cm. Capacitors were formed with either Al contacts deposited by evaporation or Pt contacts deposited by magnetron sputtering over a mask with 2×10^{-3} cm^2 area holes. The static permittivity of the films was obtained from measurements of capacitance at 100 kHz in the accumulation regime using an ESI2150-LCR apparatus. Breakdown electrical fields were evaluated using the ramp voltage stress method to the capacitors.

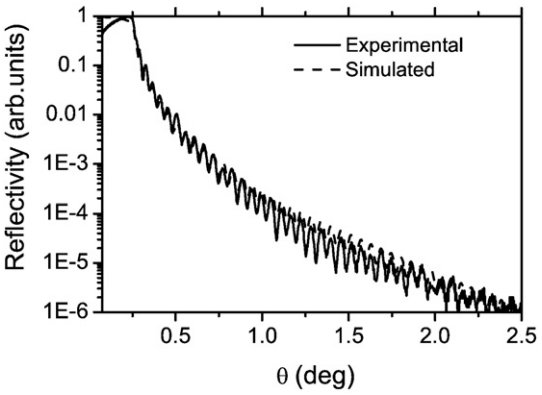

Fig. 2. XRR measurement and fit corresponding to a $Zr_xSi_{1-x}O_2$ ($x=0.55$) thin film.

3. Results

3.1. Microstructure

Fig. 1 shows a cross sectional SEM image of a typical mixed Zr–Si oxide thin film prepared by IBICVD at room temperature. This particular case corresponds to a $Zr_xSi_{1-x}O_2$ film with $x=0.3$ and thickness of 265 nm. The sample appears nearly featureless, without any clear granular or columnar structure. Standard Bragg–Brentano diffraction measurements (not shown) were consistent with a fully amorphous structure in the films.

Fig. 2 shows the XRR signal of a 75 nm thick Zr–Si–O film and the corresponding simulation. It is deduced that the density of this film is 4.1 gr/cm^3 and the interface roughness is about 0.4 nm. This analysis confirms that the substrate–film interface is rather sharp and that the films have low roughness, despite their high thickness. These results are consistent to AFM characterization of the same sample, where the root mean squared roughness obtained in a 5×5 μm image was typically below 0.2 nm.

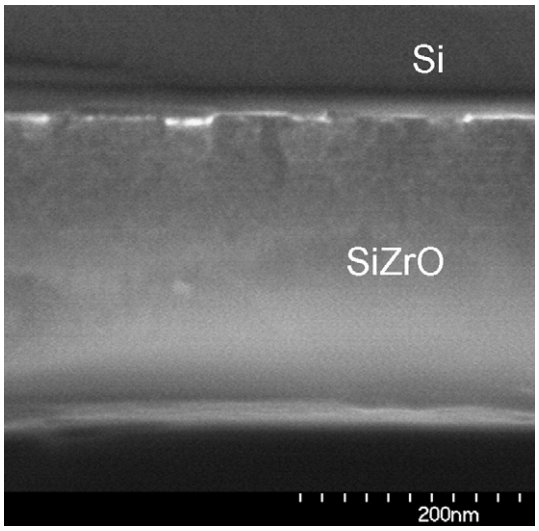

Fig. 1. Cross sectional SEM image of a mixed Zr–Si oxide prepared by IBICVD at room temperature.

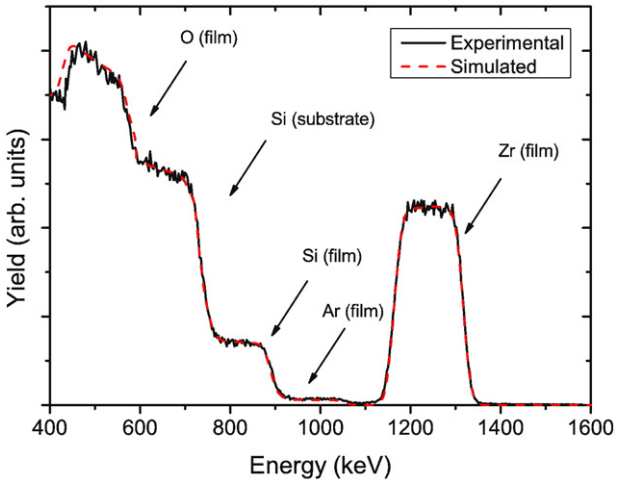

Fig. 3. RBS measurement of a $Zr_xSi_{1-x}O_2$ ($x=0.30$) thin film deposited on a Si wafer and the corresponding SIMNRA simulation.

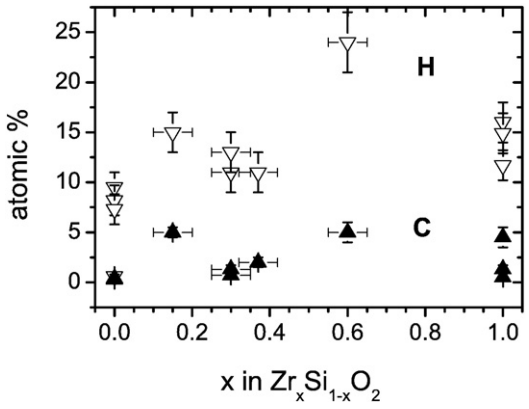

Fig. 4. H and C content as a function of the Si/Zr ratio for mixed oxides $Zr_xSi_{1-x}O_2$ ($0<x<1$) thin films prepared by IBICVD at room temperature.

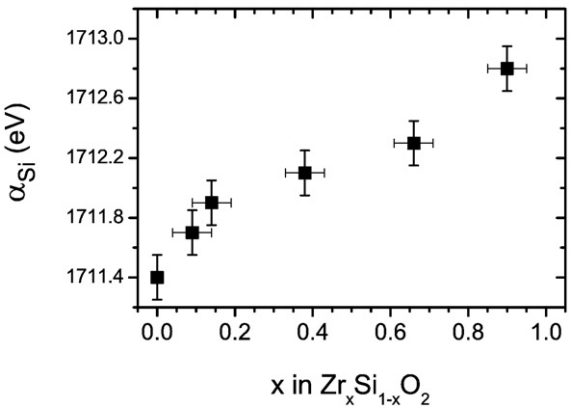

Fig. 6. Auger parameter corresponding to the Si ions in $Zr_xSi_{1-x}O_2$ thin films prepared by IBICVD at room temperature.

3.2. Composition

Fig. 3 shows a typical RBS spectrum of a Zr–Si–O thin film. In-depth distribution of the Si and Zr content was homogeneous as deduced by the flat plateau corresponding to each particular element observed in the spectrum, and also because of the consistency of the corresponding SIMNRA simulations [16]. Note that about 3–4 at.% of Ar is incorporated in the films, disregarding the Zr/Si stoichiometry. Diminishing the Ar percentage in the bombarding gas mixture below 60% produced a significant decrease (below 1 at.%) in the Ar incorporation in the films.

Fig. 4 shows the H and C content as contaminants in the mixed Zr–Si oxide thin films prepared by IBICVD as described in the experimental section. We observe that the percentage of C atoms increases by increasing the relative Zr content in the films from about 1% for pure SiO_2 to 5% for pure ZrO_2. The percentage of H atoms incorporated in the films also increases with the relative Zr content, from ~10% for samples prepared with only TrEOS precursor (i.e., $x=0$, SiO_2) to ~15% for samples prepared with only ZTB (i.e., $x=1$, ZrO_2), with a maximum (~23%) for $x=0.6$. Diminishing the Ar percentage in the bombarding gas mixture below 60% produced a significant increase of the H and C impurity content in the films.

The relative oxygen concentration (i.e., [O]/([Zr]+[Si])) was about 2.1 for the films prepared with $x=0$ and about 2.2 for those prepared with $x=1$. For intermediate stoichiometries, the relative oxygen concentration may even rise to 2.3–2.4 as for $x=0.6$–0.8 (errorbars of 5–10%).

3.3. Chemical analysis and bonding structure

Fig. 5 shows a typical XPS survey spectrum obtained from a Zr–Si–O thin film. Only Zr, Si, O and C photoelectron lines were observed. Surface stoichiometry was evaluated using suitable sensitivity factor and it was consistent with the bulk composition determined by IBA analysis. It is worth mentioning the presence of some carbon contamination (–C–, $–CH_x$ and –C=O) groups as can be observed in the inset of Fig. 5.

It is also worth mentioning that the binding energy of the Si *2p* photoemission peaks and the kinetic energy of the Si *KLL* Auger emission peaks varied with the Zr/Si composition in the films. As a result, the characteristic Auger parameters of Si in the $Zr_xSi_{1-x}O_2$ oxides varied with stoichiometry as depicted in Fig. 6. The variation of the Auger parameter of a cation with a fix oxidation state is a measure of the change local polarizability at the cation sites [17], thus indicating an evolution in the electronic structure of the material formed.

Fig. 7 shows FTIR absorbance spectra of a series of samples. Signal coming from the excitation of Si–O–Si bond type is clearly identified in pure SiO_2 and in the films with Zr content below 20% atomic ($x<0.2$). As the amount of Zr incorporated in the films increases, first a new band at 960 cm^{-1} corresponding to the excitation of Zr–O–Si bonds can be easily identified. For Zr content higher than 40% ($x>0.4$) a new band at ~390 cm^{-1} starts to be apparent. This last band is very wide and shifts to ~410 cm^{-1} for the films prepared with ZTB precursor alone (i.e., ZrO_2), indicating a change in the local bonding structure.

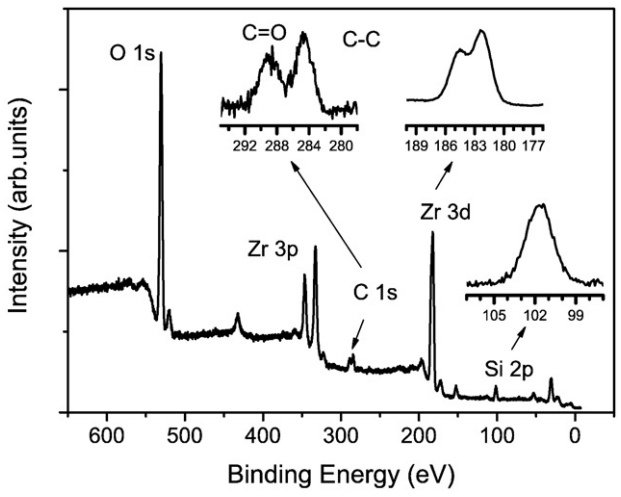

Fig. 5. XPS spectrum of a typical Zr–Si–O oxide prepared by IBICVD at room temperature.

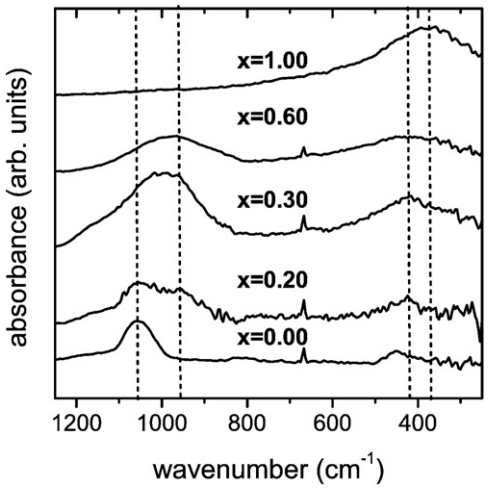

Fig. 7. Absorbance FTIR measurements on several $Zr_xSi_{1-x}O_2$ thin films deposited on Si wafers.

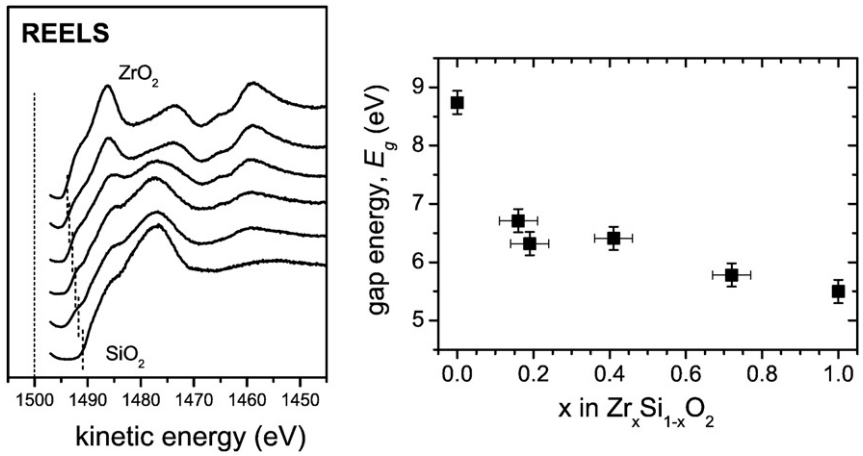

Fig. 8. Left: REELS spectra of Zr–Si mixed oxide thin films normalized to the elastic peak intensity. Right: corresponding band gap energy of the $Zr_xSi_{1-x}O_2$ thin films.

3.4. Band gap energy

Fig. 8 (left) shows a series of raw REELS spectra acquired with 1500 eV primary electrons corresponding to Zr–Si–O films. The spectra have been normalized to the same elastic peak area. Note that the threshold of absorption shifts to higher energy losses as the relative Zr content in the films decreases. Interpretation of the different features observed in the spectra for the pure oxides can be found elsewhere [18,19]. Detailed interpretation of the electronic structure of the mixed oxides will be presented in a forthcoming publication. To identify the gap energy for the measured samples, we have evaluated the absorption coefficient from the analysis of the REELS spectra of the Zr–Si–O films using OPTEELS software. Fig. 8 (right) shows E_g for different Zr/Si composition. The single oxides present E_g of 9.0 eV and 5.1 eV for SiO_2 and ZrO_2, respectively. These values agree with those found by other authors [20,21]. A sharp decrease of E_g is observed when a little amount of Zr is added to SiO_2 in the mixed Zr–Si oxides (note that $E_g = 6.0$ eV for $x = 0.15$). For films with higher Zr content ($x > 0.15$) a smooth linear decrease of E_g with x to the value of ZrO_2 is observed.

3.5. C–V measurements: permittivity, fixed charge and midgap interface state densities

Fig. 9 shows a typical high frequency (100 kHz) capacitance–voltage behavior obtained for a mixed Zr–Si oxide thin films, normalized for capacitance in the accumulation regime. The three typical regions (accumulation, depletion and inversion) from a MOS capacitor can be clearly identified. The shoulder at −1.5 V, before reaching the inversion region, is due to a high concentration of midgap interface states [22]. The midgap interface state density D_{it} evaluated from conductance measurements [22,23]indicates that $D_{it} \sim 10^{11} cm^{-2} eV^{-1}$ for $Zr_xSi_{1-x}O_2$ thin films with $x < 0.15$, and $D_{it} \sim 10^{13} cm^{-2}\ eV^{-1}$ for $0.15 < x < 0.30$. D_{it} increases for films with $x > 0.30$, with a significant distortion of the typical C–V characteristic of a MOS structure.

Values for the fixed charge Q_{eff} in the dielectric oxide can be obtained according to the expression [24]

$$Q_{eff} = C_0 \cdot (\Delta\phi_{ms} - V_{FB}) \quad (1)$$

where V_{FB} is the flat band potential, $\Delta\phi_{ms}$ is the metal-semiconductor work function difference and C_0 is the capacitance in the accumulation regime. The flat band potential V_{FB} values were evaluated using Ricco's method [25]. It was obtained that Q_{eff} for the series of mixed Zr–Si oxide dielectrics varies between $\sim 3 \times 10^{10}\ cm^{-2}$ for SiO_2 films and $\sim 2 \times 10^{12}\ cm^{-2}$ for ZrO_2 films.

The static permittivity k was evaluated from the capacitance in the accumulation regime. Fig. 10 shows k corresponding to $Zr_xSi_{1-x}O_2$ ($0 < x < 1$) thin films. It varies from 3.5–4.0 for SiO_2 to 8–10 for $x = 0.2$. Then, k remains approximately constant within the uncertainties of the measurements up to $x = 0.6$. For higher Zr concentration in the films, k increases again to ~15 for pure ZrO_2. It is worth mentioning here that, in general, and for samples with the same stoichiometry, films with higher k were prepared with a higher $P_{Ar}/(P_{O2} + P_{Ar})$ ratio. Thus, for example, it was found that k varied form 7.9 to 9.0 for $Zr_xSi_{1-x}O_2$ films with $x = 0.6$ and from 11.2 to 15.6 for ZrO_2 (films with similar thickness). The permittivity values calculated for the samples with high Zr content

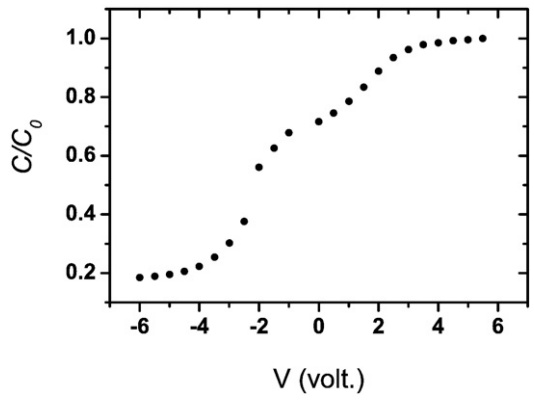

Fig. 9. Typical capacitance–voltage C–V characteristic obtained for the Zr–Si mixed oxides prepared by IBICVD at room temperature.

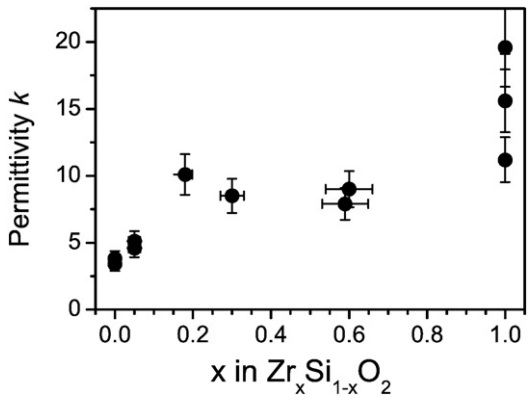

Fig. 10. Static permittivity of $Zr_xSi_{1-x}O_2$ ($0 < x < 1$) thin films prepared by IBICVD at room temperature.

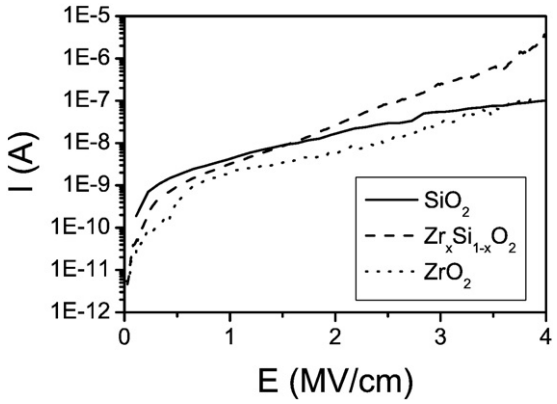

Fig. 11. I–V characteristics of $Zr_xSi_{1-x}O_2$ ($0<x<1$) thin films prepared by IBICVD at room temperature.

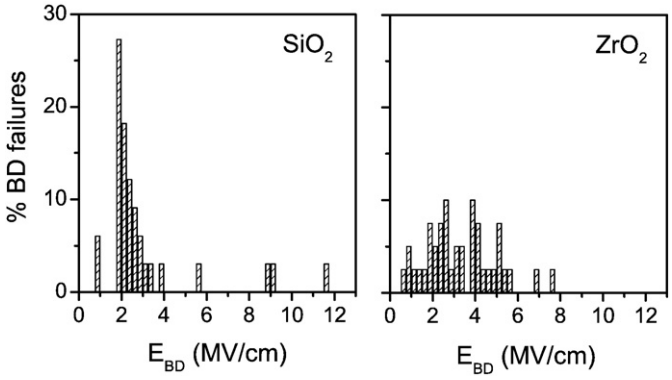

Fig. 13. Statistics of electric field breakdown on SiO_2 (left) and ZrO_2 (right) thin films prepared by IBICVD at room temperature.

should be considered with caution due to the high midgap state density and the distorted capacitance–voltage behaviour.

3.6. I–V measurements: current conduction mechanisms and dielectric breakdown

We have studied the current conduction mechanism taking place in the mixed Zr–Si oxide samples before dielectric breakdown. Fig. 11 shows the I–V characteristics obtained for the capacitors. It is observed, as a general behavior, a change in slope between low and high electric field applied to the capacitors. Several conduction mechanisms have been proposed to describe charge transport in dielectric films [26]. Among them, Schottky and Poole-Frenkel emission are usually considered for highly defective films with trap energy levels in the insulator band gap [27]. The dependence of the current density (J_{Sh} or $J_{P\text{-}F}$) with the applied electric field *E, for these mechanisms,* is described by the following expressions

$$ln[J_{Sh}] = Cte + \frac{1}{K_B T}\sqrt{\frac{q^3 E}{4\pi\varepsilon_0 k}} \tag{2}$$

$$ln\left[\frac{J_{P-F}}{E}\right] = Cte' + \frac{1}{rK_B T}\sqrt{\frac{q^3 E}{4\pi\varepsilon_0 k}} \tag{3}$$

where, ε_0 is the vacuum dielectric constant, q is the electron charge, K_B is the Boltzmann constant, and T is the temperature. The factor r takes values between 1 and 2 depending on the Fermi level position. In case of high number of traps, it is recommended to take $r=2$ [28].

It is found that the I–V characteristic obtained in the films is consistent to Schottky emission in the low electric field region (between 0.2 MV/cm and 0.5 MV/cm) and to Poole-Frenkel emission in the high electric field region (between 2.0 MV/cm and 4.0 MV/cm). Fig. 12 shows examples of current–voltage fits obtained with Eqs. (2) and (3) below. Although temperature dependent measurements were not performed to confirm the conduction mechanisms described avobe, it is worth mentioning that the values of k obtained to get these fits were in agreement with those obtained from the capacitance measurements in the accumulation regime.

The dielectric strength of an oxide layer depends on the properties of the oxide material (i.e., electronic structure, band gap energy) and their microstructure (degree of crystallization, presence of defects, etc). It is often expressed in terms of the electric field at which the insulator is irreversibly damaged and has lost its insulating properties. In practice, it means that a certain density current overcomes a threshold [29]. In our case, and based on the behaviour of most of the prepared films, this threshold has been taken as 10^{-3} A/cm^2. Breakdown is defined intrinsic when it is related only to the oxide electronic structure and extrinsic when it is due to defects.

Dielectric damage or breakdown (DB) of an insulator oxide thin film is due to interface trap generation initiated by the energy loss of injected electrons and holes due to the action of the applied electrical field. DB is a statistical phenomenon: for two identical devices subjected to the same stress, breakdown is caused at different times. Therefore it can only be described in statistical terms. Fig. 13 shows the typical statistical behavior observed for the breakdown electrical field E_{BD} for different stoichiometries. We observe a wide distribution of breakdown electrical field. The maximum values of E_{BD} decrease from ~10 MV/cm for SiO_2 to ~5 MV/cm for ZrO_2.

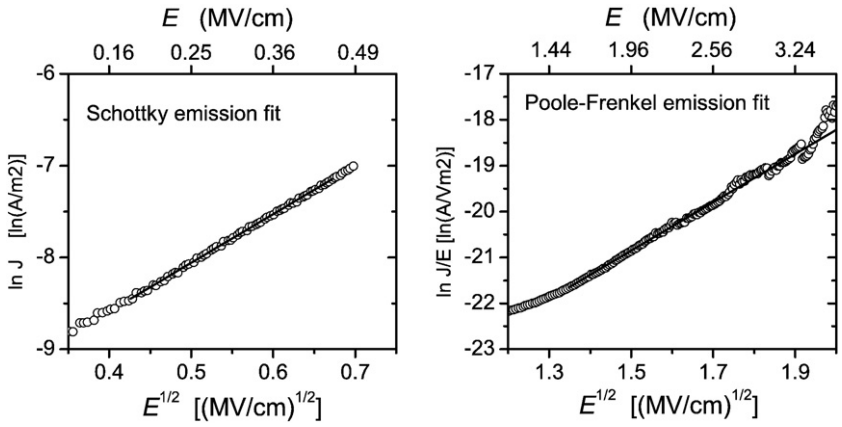

Fig. 12. Current–voltage fits to Schottky (left) and Poole-Frenkel (right) emission at low and high electric fields, respectively.

4. Discussion

The $Zr_xSi_{1-x}O_2$ ($0<x<1$) thin films prepared by IBICVD at room temperature using O_2/Ar mixtures as bombarding gas are predominantly amorphous as deduced from SEM, X-Ray diffraction and FTIR characterization. Ballistic effects at the surface of the growing films contribute to increase the disorder during growth and therefore to the formation of amorphous structures. The incorporation of Ar atoms within the structure during growth also supports this finding.

The mixed Zr–Si oxide thin films were flat as previously observed by AFM and SEM for the single oxides [6–8]. The substrate-film interface is rather sharp, despite the use of ion beams of 400 eV for the decomposition of the volatile precursors. Based on TRIM calculations [30] a penetration depth of ~2.0 nm is expected for the Ar^+/O_2^+ 400 eV ion mixture that is consistent with the interface roughness deduced from the XRR simulations.

Phase segregation does not take place for intermediate Zr/Si compositions as deduced from FTIR and XPS characterization. Regarding FTIR spectra of samples with intermediate stoichiometries, three facts support that idea: the presence of the new Si–O–Zr band, the strong diminishing of the Si–O–Si band, and the broad Zr–O–Zr band at 300–500 cm^{-1} [31]. The Si–O–Zr band shifts depending on the Zr content in the films. On the other hand, the smooth variation of the Auger parameter with the stoichiometry also sustains this finding [32].

Although a systematic study of the stability of the films is not performed, it has been evidenced that the Ar incorporated in the Zr–O–Si network of the films is not released after annealing at 300°C for any x composition. On the other hand, it has been previously observed that the crystallization of ZrO_2 films is strongly influenced by the presence of the Ar within the initial amorphous structure, and that these Ar atoms do not disappear after heavy annealing at 800 °C [8,33,34].

In a previous work it was shown that carboxylic and hydroxyl groups are incorporated into the zirconium silicate thin films [35]. This is corroborated by the IBA analysis. Incorporation of these impurities in the films is less favored when the Ar content in the bombardment gas mixture is increased. A possible explanation for this effect might be that there is a threshold momentum that prevents the incorporation of these groups to the films (note that the momentum transferred by 400 eV Ar^+ ions to the atoms at the film surface is more than twice that transferred by 400 eV O_2^+ ions [36]). Another explanation might be the fact that the relative amount of atomic O^+ with respect to O_2^+ increases in a O_2/Ar RF plasma with respect to a O_2 RF plasma [37], because the ionization efficiency of a O_2 molecule in the later is lesser than that in the former. Thus, the chemical reactivity of the bombarding gas would be increased, producing more complete oxidation of the ZTB precursor. Carboxylic groups are not reported in zirconia and zirconium silicates thin films prepared by thermal decomposition of the ZTB precursor [31,38], but the presence of C=O species is found in films prepared by the decomposition of ZTB by microwave plasma [12,39]. In fact, we have observed that the carboxylic groups are weakly linked to the film structure because they can be easily released after annealing at 300 °C.

The variation of the band gap also supports the idea of a continuous evolution between SiO_2 to ZrO_2 material. The band gap decreases drastically for very low content of Zr. This effect has been justified previously by the presence of Si–O–Zr bond structures according to quantum mechanical calculations [32]. Similar behavior is observed in Si–Ti–O films [10].

It has been obtained a high level of midgap interface states in the formed MOS structures that explains the distortions of the C–V characteristics for films with $x>0.2$. We can justify the increase in D_{it} and Q_{eff} with increasing amount of impurities incorporated in the films.

It is observed a non-linear correlation between stoichiometry and permittivity for the mixed Zr–Si oxide thin films described in this work. This behaviour has been previously reported for zirconium silicates with $x<0.5$ [2,3]. It has been related to the change in coordination of Zr^{4+} cations between 4 for $x<0.1$ to 8 for $x>0.5$ [38]. In the case of the amorphous Zr–Si–O system, bond order (defined as the ratio of number of valence electrons available from each Zr atom to the number of O-atoms nearest neighbors) varies between 1 for Zr diluted in a SiO_2 matrix to 0.5 present in $ZrSiO_4$ and ZrO_2. This change of coordination in amorphous Zr silicates has been confirmed by extended X-ray absorption fine structure studies [38]. Changes in the ionic and polar contributions to the static permittivity are very sensitive to local order, and therefore, this would justify the different behavior of the static permittivity with the stoichiometry of the films. It is worth mentioning that our results are in contradiction to others [40] where by increasing the O_2 content in the O_2/Ar mixture, higher permittivity and lower interfacial trap density were observed when ZrO_2 was deposited at room temperature by plasma decomposition of ZTB.

The low values of breakdown electrical field for Zr–Si–O thin films prepared by IBICVD are also justified by the presence of high concentration of –C–H and –C=O impurities. Note, for example, that the permittivity and the breakdown electrical field of compact SiO_2 and ZrO_2 thin films reported in the literature could be as high as 15–17 [41] and 5.6–6.0 MV/cm [42] respectively. Note, in addition, that films with highest H and C content, as those prepared with low Ar content in the bombarding gas mixture showed, $E_{BD}<1.0$ MV/cm. Similar results were obtained when bombarding ions with lower kinetic energy (200 eV) were used.

5. Conclusions

We have reported on the electrical characteristics of $Zr_xSi_{1-x}O_2$ dielectric thin films prepared by IBICVD at room temperature using mixtures of Ar^+/O_2^- ions of 400 eV. The films were amorphous and flat. The content of impurities such as H (10–23 at.%) and C (1–5 at.%) increased with the amount of Zr in the films. A 3–4 at.% of Ar atoms is incorporated in the films disregarding the Zr/Si content. No phase segregation of the pure single oxides is observed.

It is found that the midgap interface state density and the fixed charge in the oxide film increase with the Zr and impurities content. The former increases from ~10^{11} cm^{-2} eV^{-1}, for films with $x<0.15$, to ~10^{13} cm^{-2} eV^{-1}, for $0.15<x<0.30$, and takes larger values for $x>0.30$, affecting significantly the measured C–V characteristic of the MOS structures. The later increases from ~3×10^{10} cm^{-2} for SiO_2 films to ~2×10^{12} cm^{-2} for ZrO_2. The static permittivity of the films shows a rapid increase from values about 3.5–4.0 in the case of SiO_2 films to about 10 for $0.2<x<0.6$. This is justified by the change in coordination of the Zr ions when diluted in a silica matrix.

Rapid decrease of the band gap is obtained for small amount of Zr incorporated in the films. It is found that the conduction mechanism in the low electric field region (i.e., 0.2–0.5 MV/cm) is Schottky emission while in the high electric field region (i.e., 2.0–4.0 MV/cm) is Poole-Frenkel emission disregarding the Zr/Si stoichiometry. The oxide films are characterized by extrinsic dielectric breakdown. A large dispersion in the breakdown electrical field is observed, that is justified by the large density of point defects present in the deposited dielectric oxides. The maximum electrical field breakdown decreases from ~10 MV/cm for pure SiO_2 to ~5 MV/cm for ZrO_2 films.

Acknowledgments

We thank the Spanish Ministry of Science and Education for financial support (grants no. MAT 2004-01558 and MAT2007-65764).

References

[1] S.J. Wang, C.K. Ong, S.Y. Xu, P. Chen, W.C. Tjiu, J.W. Chai, A.C.H. Huan, W.J. Yoo, J.S. Lim, W. Feng, W.K. Choi, Appl. Phys. Lett. 78 (2001) 1604.
[2] G.D. Wilk, R.M. Wallace, Appl. Phys. Lett. 76 (2000) 112.
[3] G.D. Wilk, R.M. Wallace, J.M. Anthony, J. Appl. Phys. 87 (2000) 484.
[4] A. Javey, H. Kim, M. Brink, Q. Wang, A. Ural, J. Guo, P. McIntyre, P. McEuen, M. Lundstrom, H. Dai, Nat. Mater. 1 (2002) 241.

[5] A.R. González-Elipe, F. Yubero, J.M. Sanz, Low Energy Ion Assisted Film Growth, Imperial College Press, 2003, p. 58.
[6] A. Barranco, F. Yubero, J. Cotrino, J.P. Espinós, J. Benítez, T.C. Rojas, J. Allain, T. Girardeau, J.P. Riviere, A.R. González-Elipe, Thin Solid Films 396 (2001) 9.
[7] A. Barranco, F. Yubero, J.P. Espinós, J. Benítez, A.R. González-Elipe, J. Cotrino, J. Allain, T. Girardeau, J.P. Riviere, Surf. Coat. Technol. 142–144 (2001) 856.
[8] J.P. Holgado, J.P. Espinós, F. Yubero, A. Justo, M. Ocaña, J. Benítez, A.R. González-Elipe, Thin Solid Films 389 (2001) 34.
[9] F. Yubero, A. Stabel, A.R. González-Elipe, J. Vac. Sci. Technol. A 16 (1998) 3477.
[10] F. Gracia, F. Yubero, J.P. Holgado, J.P. Espinós, A.R. González-Elipe, T. Girardeau, Thin Solid Films 500 (2006) 19.
[11] W. Kim, S. Kang, S. Rhee, J. Vac. Sci. Technol. A 21 (2003) L16.
[12] B. Cho, S. Lao, L. Sha, J.P. Chang, J. Vac. Sci. Technol. A 19 (2001) 2751.
[13] V. Drinek, Z. Bastl, J. Subrt, J. Pola, Appl. Surf. Sci. 108 (1997) 283.
[14] A.R. González-Elipe, J.P. Espinós, A. Barranco, F. Yubero, A. Caballero, J. Phys. IV 9 (1999) 699.
[15] OPTEELS software. Available on the web (http://sincaf-icmse.es/en/topicsofinterest); 2006.
[16] M. Mayer, in: J.L. Duggan, I.L. Morgan (Eds.), SIMNRA, a Simulation Program for the Analysis of NRA, RBS and ERDA, Proceedings of the 15th International Conference on the Application of Accelerators in Research and Industry, American Institute of Physics Conference Proceedings, vol. 475, 1999, p. 541.
[17] A.R. González-Elipe, F. Yubero, in: H.S. Nalwa (Ed.), Spectroscopic Characterization of Oxide/Oxide Interfaces, Handbook of Surfaces and Interfaces of Materials, vol. 2, Academic Press, San Diego, 2001, p. 147.
[18] P. Prieto, F. Yubero, E. Elizalde, J.M. Sanz, J. Vac. Sci. Technol. A 14 (1996) 3181.
[19] F. Yubero, S. Tougaard, E. Elizalde, J.M. Sanz, Surf. Interface Anal. 20 (1993) 719.
[20] L.A.J. Garvie, P. Rez, J.R. Alvarez, P.R. Busek, Solid State Commun. 106 (1998) 303.
[21] F. Yubero, J.M. Sanz, J.F. Trigo, E. Elizalde, S. Tougaard, Surf. Interface Anal. 22 (1994) 124.
[22] R.J. Carter, E. Cartier, A. Kerber, L. Pantisano, T. Schram, S. De Gendt, M. Heyns, Appl. Phys. Lett. 83 (2003) 533.
[23] W.A. Hill, C.C. Coleman, Solid-St. Electron. 23 (1980) 987.
[24] S.M. Sze, Physics of Semiconductor Devices, 2nd ed.Wiley, New York, 1981.
[25] B. Ricco, P. Olivo, T.N. Nguyen, T.S. Kuan, G. Ferriani, IEEE Trans. Electron Devices 35 (1988) 432.
[26] P. Gonon, A. Deneuville, F. Fontaine, E. Gheeraert, J. Appl. Phys. 78 (1995) 6633.
[27] J.P. Chang, Y.S. Lin, Appl. Phys. Lett. 79 (2001) 3666.
[28] J.R. Yeargan, H.L. Taylor, J. Appl. Phys. 39 (1968) 5600.
[29] J.F. Verweij, J.H. Klootwijk, Microelectron. J. 27 (1996) 611.
[30] J.F. Ziegler, J.P. Biersack, U. Littmark, The Stopping and Range of Ions in Solids, vol. 1, Pergamon, 1985.
[31] G. Lucovsky, G.B. Rayner, D. Kang, C.L. Hinkle, J.G. Hong, Appl. Surf. Sci. 234 (2004) 429.
[32] F.J. Ferrer, F. Yubero, J.A. Mejías, J. García-López, A.R. González-Elipe, J. Appl. Phys. 102 (2007) 084112.
[33] F. Yubero, M. Ocaña, A. Caballero, A.R. González-Elipe, Acta Mater. 48 (2000) 4555.
[34] A.R. Gonzalez-Elipe, F. Yubero, J.P. Espinós, A. Caballero, M. Ocaña, J.P. Holgado, J. Morales, Surf. Coat. Technol. 125 (2000) 116.
[35] F.J. Ferrer, F. Frutos, J. García-López, A.R. González-Elipe, F. Yubero, Thin Solid Films 516 (2007) 481.
[36] M. Alvisi, S. Scaglione, S. Martelli, A. Rizzo, L. Vasanelli, Thin Solid Films 354 (1999) 19.
[37] A. Yanguas-Gil, J. Cotrino, A.R. González-Elipe, J. Phys. D: Appl. Phys. 40 (2007) 3411.
[38] G. Lucovsky, G.B. Rayner Jr., Appl. Phys. Lett. 77 (2000) 2912.
[39] L. Koltunski, R.A.B. Devine, Appl. Phys. Lett. 79 (2001) 320.
[40] B. Cho, J. Wang, L. Sha, J.P. Chang, Appl. Phys. Lett. 80 (2002) 1052.
[41] D.H. Kuo, C.H. Chien, C.H. Huang, Thin Solid Films 420–421 (2002) 47.
[42] J. Niinistö, M. Putkonen, L. Niinistö, K. Kukli, M. Ritala, M. Leskelä, J. Appl. Phys. 95 (2004) 84.